

# Nonlocal Excitation Spectra in 2D Doped Hubbard Model

Yoshiro KAKEHASHI<sup>1\*</sup> and Peter FULDE<sup>2†</sup>

<sup>1</sup>*Department of Physics and Earth Sciences, Faculty of Science, University of Ryukyus,  
1 Senbaru, Nishihara, Okinawa, 903-0213, Japan*

<sup>2</sup>*Max-Planck-Institut für Physik komplexer Systeme, Nöthnitzer Str. 38, D-01187 Dresden, Germany*

Single-particle excitation spectra of the two-dimensional Hubbard model on the square lattice near half filling and at zero temperature are investigated on the basis of the self-consistent projection operator method. The method guarantees a high accuracy of the spectra with high energy and high momentum resolutions. It takes into account long-range intersite correlations as well as the strong on-site correlations. Effects of nonlocal excitations are clarified by comparing the results with those of the single-site approximation. The calculated spectra verify the quantum Monte-Carlo results for finite temperatures. The spectra at the Fermi level yield a hole-like Fermi surface in the underdoped region and an electron-like Fermi surface in the overdoped region. From a numerical analysis of the momentum dependent effective mass and self-energy, it is concluded that a marginal Fermi-liquid like state persists even at finite doping concentrations in the strongly correlated region because a van Hove singularity is pinned to the Fermi surface. It is also found that a kink structure appears in the quasiparticle energy band in the same region. The kink is shown to be caused by a mixing between the quasiparticle band and an excitation band with strong short-range antiferromagnetic correlations. These results suggest an explanation for some of the unusual properties of the normal state in high- $T_c$  cuprates.

KEYWORDS: quasiparticle excitations, two-dimensional Hubbard model, momentum-dependent self-energy, marginal Fermi liquid, ARPES, kink, cuprate, LSCO

## 1. Introduction

The two-dimensional (2D) Hubbard model has been widely investigated in the past two decades because it has been the simplest model for describing the high-temperature superconductivity in layered Cu-based perovskites.<sup>1-3</sup> The Cu  $3d_{x^2-y^2}$  orbitals on a square lattice hybridize with the O  $2p_x$  and  $2p_y$  orbitals on the  $\text{CuO}_2$  plane and form an antibonding band near the Fermi level. There is a strong on-site Coulomb repulsion of electrons in hybridized Cu  $3d$  orbitals with different spins, which leads to the 2D Hubbard model.<sup>4-6</sup>

The 2D Hubbard model at half-filling with nearest-neighbor electron hopping is an antiferromagnetic insulator with the Néel temperature  $T_N = 0$  according to the Mermin-Wagner theorem.<sup>7</sup> When holes are doped, charge fluctuations counteract antiferromagnetism and a metallic state should be realized. Rigorous results are however scarce especially for intermediate Coulomb interaction strengths, and therefore the model is of current interest in condensed matter physics.

Numerical techniques applied to the doped regime such as the Lanczos method<sup>1</sup> and Quantum Monte-Carlo (QMC)<sup>8-10</sup> have verified the formation of a gap at half-filling and clarified global features of excitation spectra from the insulator to a metal. The antiferromagnetic correlations have been shown to reduce rapidly with increasing hole concentration.<sup>10,11</sup> More recent calculations based on the dynamical cluster approximation<sup>12</sup> verified a hole-like Fermi surface in the underdoped re-

gion and an electron-like Fermi surface in the overdoped region.<sup>13</sup> The calculations also suggested the possibilities of a pseudogap state as well as the occurrence of superconductivity.<sup>14</sup>

The methods mentioned above are based on a cluster approach. The approach treats a finite cluster explicitly by assuming a boundary condition, or implicitly by embedding it in an effective medium. Since it is numerically not possible to treat a large cluster, finite size effects are inevitable in these methods. In fact, the methods do not yield high momentum and energy resolutions for excitation spectra, and do not describe the long-range intersite correlations due to finite cluster size.<sup>15</sup> It is difficult to achieve a momentum resolution better than  $0.005 \text{ \AA}^{-1}$  which was recently obtained in angle resolved photoemission spectroscopy (ARPES).<sup>16</sup> This difficulty becomes serious for the investigations of the kink structure of the quasiparticle band found in the cuprates. Therefore one needs different approaches to study a more detailed structure of spectra in the 2D Hubbard model.

In this paper we investigate the single-particle excitation spectra and related properties of the 2D Hubbard model on the square lattice by making use of the self-consistent projection operator method (SCPM).<sup>17</sup> The SCPM is an extension of the projection operator method which uses the coherent potential approximation (PM-CPA),<sup>18</sup> when determining the momentum dependent self-energy. The SCPM treats directly the retarded Green function, describes the local on-site correlations by using an effective medium, and takes into account the intersite correlations up to infinity by using an incremental cluster expansion.<sup>19,20</sup> Thus the method yields high momentum

\*E-mail address: yok@sci.u-ryukyuu.ac.jp

†E-mail address: fulde@mpipks-dresden.mpg.de: to be published in J. Phys. Soc. Jpn. Vol. 76, No. 7 (2007)

and energy resolutions, and allows us to determine the detailed structure of nonlocal excitations in both momentum and energy spaces. Using the SCPM, we will reveal the nonlocal effects on the excitation spectra of the 2D Hubbard model and its momentum dependent properties at zero temperature, which could not be clarified by means of the other methods.

The high- $T_c$  cuprates have unusual properties in the normal state; the resistivity shows a  $T$ -linear temperature dependence and a temperature independent term appears in the nuclear relaxation rate.<sup>21</sup> These features were first explained by a phenomenological marginal Fermi liquid (MFL) scenario.<sup>22</sup> The MFL is defined by electrons whose imaginary part of the self-energy near the Fermi surface,  $\text{Im}\Sigma(\omega, T)$  is proportional to  $|\omega|$  instead of  $\omega^2$  where  $\omega$  ( $> T$ ) is an excitation energy and  $T$  is the temperature. Accordingly,  $\text{Re}\Sigma(\omega, T) \propto \omega \ln|\omega|$ . In spite of successes of the theory, the MFL has remained puzzling because no microscopic theory could be provided for it. We show in the present paper that a MFL like behavior appears in the underdoped region, which may be considered as a form of justification of the phenomenological MFL theory.

Another interesting point of our results is that a kink structure in the quasiparticle band appears in the underdoped region. Recent ARPES experiments have revealed a kink in the quasiparticle band of high- $T_c$  cuprates in both the normal and superconducting state.<sup>23–25</sup> The typical kink energy at which the quasiparticle velocity changes is 70 meV. Previous theories for the kink structure assumed either a coupling of electrons to a magnetic resonance mode found in inelastic neutron scattering experiments<sup>16,26</sup> or a coupling to a longitudinal optical phonon mode.<sup>25,27</sup> These theories do not take into account other electron correlations which are an essential ingredient of the high- $T_c$  cuprates. We demonstrate on the basis of the SCPM that the kink structure can be explained by electron correlations without introducing lattice degrees of freedom. This provides a new possible mechanism for the observed kink structure in cuprates. Preliminary results on these topics have been published recently.<sup>28,29</sup> It should be noted that the validity of numerical calculations on these problems strongly depends on the momentum and energy resolutions. We therefore have recalculated the spectra increasing the number of mesh from  $80 \times 80$  to  $160 \times 160$  in the first Brillouin zone and the energy mesh by a factor of two. On the basis of the new results of calculations we will discuss in the present paper the MFL and the kink structure in more details.

The paper is organized as follows. In the next section, we review briefly the SCPM to the Hubbard model. In Sec. III we present our results of calculations for the excitation spectra. We limit ourselves here to excitation spectra in the normal state at zero temperature. In Sec. III A we discuss the characteristics of the excitation spectra at half-filling under the assumption of a paramagnetic effective medium. In Sec. III B, we treat the doped case. We present the excitation spectra, integrated density of states (DOS), Fermi surface, momentum distribution, and the momentum dependent effective mass. We clar-

ify the nonlocal effects of electron correlations on these quantities by comparing them with those of the single-site approximation (SSA) and other numerical results. The MFL-like behavior which we find in the underdoped region is discussed separately in Sec. III C. The MFL features are shown to be caused by a pinning of the van Hove singularity to the Fermi surface under doping. In Sec. III D, we discuss the kink structure of the quasiparticle band, which is obtained in the underdoped region. The results of our calculations are summarized in Sec IV, where also the unusual behavior of cuprates in the normal state is discussed.

## 2. Self-consistent projection operator method

We consider a Hubbard model on a square lattice with an atomic level  $\epsilon_0$ , a nearest-neighbor transfer integral  $t_{ij}$  ( $= t$ ), and an on-site Coulomb interaction parameter  $U$ .

$$H = \sum_{i,\sigma} (\epsilon_0 - \mu) n_{i\sigma} + \sum_{i,j,\sigma} t_{ij} a_{i\sigma}^\dagger a_{j\sigma} + U \sum_i n_{i\uparrow} n_{i\downarrow}. \quad (1)$$

Here the chemical potential  $\mu$  has been added to the Hamiltonian. Furthermore  $a_{i\sigma}^\dagger$  ( $a_{i\sigma}$ ) is the creation (annihilation) operator for an electron with spin  $\sigma$  on site  $i$  and  $n_{i\sigma} = a_{i\sigma}^\dagger a_{i\sigma}$ .

The single-particle excitation spectrum is obtained from the poles of the retarded Green function given by

$$G_{k\sigma}(z) = \frac{1}{z - \epsilon_{k\sigma} - \Lambda_{k\sigma}(z)}. \quad (2)$$

Here  $z = \omega + i\delta$  with  $\delta$  being an infinitesimal positive number,  $\epsilon_{k\sigma}$  is the Hartree-Fock energy given by  $\epsilon_{k\sigma} = \epsilon_0 + \epsilon_k - \mu + U\langle n_{i-\sigma} \rangle$  where  $\langle n_{i\sigma} \rangle$  and  $\epsilon_k$  denote the average number of electrons with spin  $\sigma$  on site  $i$  and the dispersive part of the energy band for noninteracting electrons, respectively.

The self-energy  $\Lambda_{k\sigma}(z)$  is given by a Fourier transform of the memory function  $M_{j\sigma}(z)$  as

$$\Lambda_{k\sigma}(z) = U^2 \sum_j M_{j0\sigma}(z) \exp(i\mathbf{k} \cdot \mathbf{R}_j). \quad (3)$$

In the projection operator method,<sup>30–32</sup> the memory function is given by

$$M_{ij\sigma}(z) = \left( A_{i\sigma}^\dagger \left| (z - \bar{L})^{-1} A_{j\sigma}^\dagger \right. \right). \quad (4)$$

Here  $A_{i\sigma}^\dagger = a_{i\sigma}^\dagger (n_{i-\sigma} - \langle n_{i-\sigma} \rangle)$ . The inner product of operators  $A$  and  $B$  is defined by  $(A|B) = \langle [A^+, B]_+ \rangle$  where the expectation value is taken with respect to the ground state of the system. The dynamics of the electronic system is described by a superoperator  $L$ . It acts on other operators  $A$  according to  $LA = [H, A]_-$ . Furthermore  $\bar{L} = QLQ$  where the projector  $Q$  is given by  $Q = 1 - P$  and  $P = \sum_{i\sigma} |a_{i\sigma}^\dagger\rangle \langle a_{i\sigma}^\dagger|$ . Thus  $Q$  eliminates  $|a_{i\sigma}^\dagger\rangle$  from further considerations.

In the SCPM<sup>17</sup> we introduce an effective Liouville operator

$$\tilde{L}(z)A = [\tilde{H}(z), A]_- , \quad (5)$$

$$\tilde{H}(z) = H_0 + \sum_{i\sigma} \tilde{\Sigma}_\sigma(z) n_{i\sigma} . \quad (6)$$

Here  $H_0$  is the Hartree-Fock Hamiltonian, and  $\tilde{\Sigma}_\sigma(z)$  defines an energy-dependent effective medium and is called the coherent potential. The Liouvillean  $L$  is divided into a coherent part  $\tilde{L}(z)$  and an interaction part  $L_I(z)$ . By making use of the multiple scattering theory, we can derive an incremental cluster expansion for the memory functions:

$$M_{ii\sigma}(z) = M_{ii\sigma}^{(i)}(z) + \sum_{l \neq i} \Delta M_{ii\sigma}^{(il)}(z) + \frac{1}{2} \sum_{l \neq i} \sum_{m \neq i, l} \Delta M_{ii\sigma}^{(ilm)}(z) + \dots, \quad (7)$$

$$M_{ij\sigma}(z) = M_{ij\sigma}^{(ij)}(z) + \sum_{l \neq i, j} \Delta M_{ij\sigma}^{(ijl)}(z) + \frac{1}{2} \sum_{l \neq i, j} \sum_{m \neq i, j, l} \Delta M_{ij\sigma}^{(ijlm)}(z) + \dots, \quad (8)$$

with

$$\Delta M_{ii\sigma}^{(il)}(z) = M_{ii\sigma}^{(il)}(z) - M_{ii\sigma}^{(i)}(z), \quad (9)$$

$$\Delta M_{ii\sigma}^{(ilm)}(z) = M_{ii\sigma}^{(ilm)}(z) - \Delta M_{ii\sigma}^{(il)}(z) - \Delta M_{ii\sigma}^{(im)}(z) - M_{ii\sigma}^{(i)}(z), \quad (10)$$

$$\Delta M_{ij\sigma}^{(ijl)}(z) = M_{ij\sigma}^{(ijl)}(z) - M_{ij\sigma}^{(ij)}(z), \quad (11)$$

$$\Delta M_{ij\sigma}^{(ijlm)}(z) = M_{ij\sigma}^{(ijlm)}(z) - \Delta M_{ij\sigma}^{(ijl)}(z) - \Delta M_{ij\sigma}^{(ijm)}(z) - M_{ij\sigma}^{(ij)}(z). \quad (12)$$

In the above expressions,  $M_{ij\sigma}^{(c)}(z)$  are cluster memory functions defined by

$$M_{ij\sigma}^{(c)}(z) = \left( A_{i\sigma}^\dagger \left| (z - \bar{L}^{(c)}(z))^{-1} A_{j\sigma}^\dagger \right. \right), \quad (13)$$

$$L^{(c)}(z)A =$$

$$\left[ \tilde{H}(z) - \sum_{i \in c} \left( \sum_{\sigma} \tilde{\Sigma}_\sigma(z) n_{i\sigma} - U \delta n_{i\uparrow} \delta n_{i\downarrow} \right), A \right]_-. \quad (14)$$

Here  $\bar{L}^{(c)}(z) = QL^{(c)}(z)Q$ , and  $\delta n_{i\sigma} = n_{i\sigma} - \langle n_{i\sigma} \rangle$ .  $L^{(c)}(z)$  is the Liouvillean for the cluster  $c$  which is embedded in an effective medium  $\tilde{\Sigma}_\sigma(z)$ , and  $N_c$  denotes the number of atoms in the cluster. It should be noted that we take into account all the 'clusters' obtained by choosing any  $N_c$  sites from the 2D square lattice points. This is quite different from the usual cluster approaches in which only one compact cluster of sites with a given form is considered. It should also be noted that when the off-diagonal memory function (eq.(8)) is neglected and only the single-site term (SSA) is taken into account in eq. (7), the SCPM reduces to the PM-CPA, which is equivalent to the many-body CPA,<sup>33</sup> the dynamical CPA,<sup>34</sup> and the dynamical mean-field theory.<sup>35,36</sup>

We use here the memory functions obtained by the renormalized perturbation scheme:<sup>17</sup>

$$M_{ij\sigma}^{(c)}(z) = \left[ \mathbf{M}_0^{(c)} \cdot (1 - \mathbf{L}_I^{(c)} \cdot \mathbf{M}_0^{(c)})^{-1} \right]_{ij\sigma}. \quad (15)$$

The diagonal matrix  $\bar{\mathbf{L}}_I^{(c)}$  is defined by<sup>37</sup>

$$\bar{\mathbf{L}}_I^{(c)} = [\bar{L}_{I\sigma}^{(i)}, \bar{L}_{I\sigma}^{(j)}, \dots, \bar{L}_{I\sigma}^{(l)}], \quad (16)$$

$$\bar{L}_{I\sigma}^{(i)}(z) = \frac{U(1 - 2\langle n_{i-\sigma} \rangle)}{\langle n_{i-\sigma} \rangle (1 - \langle n_{i-\sigma} \rangle)}. \quad (17)$$

The screened memory function  $\hat{\mathbf{M}}_0^{(c)}$  in eq. (15) is a  $N_c \times N_c$  matrix given by

$$M_{0ij\sigma}^{(c)}(z) = A_{ij\sigma} \int \frac{d\epsilon d\epsilon' d\epsilon'' \tilde{\rho}_{ij\sigma}^{(c)}(\epsilon) \tilde{\rho}_{ij-\sigma}^{(c)}(\epsilon') \tilde{\rho}_{j-i-\sigma}^{(c)}(\epsilon'') \chi(\epsilon, \epsilon', \epsilon'')}{z - \epsilon - \epsilon' + \epsilon''}, \quad (18)$$

$$A_{ij\sigma} = \frac{\langle n_{i-\sigma} \rangle (1 - \langle n_{i-\sigma} \rangle)}{\langle n_{i-\sigma} \rangle_0 (1 - \langle n_{i-\sigma} \rangle_0)} \delta_{ij} + 1 - \delta_{ij}, \quad (19)$$

$$\chi(\epsilon, \epsilon', \epsilon'') = f(-\epsilon) f(-\epsilon') f(\epsilon'') + f(\epsilon) f(\epsilon') f(-\epsilon''). \quad (20)$$

The memory function  $\hat{M}_{0ij\sigma}^{(c)}$  consists of that of the second-order perturbation<sup>38,39</sup> theory and of a prefactor  $A_{ij\sigma}$  ensuring the correct second moment in the moment expansion. Furthermore  $\langle n_{i\sigma} \rangle_0$  is the average electron number defined by  $\langle n_{i\sigma} \rangle_0 = \int d\omega f(\omega) \tilde{\rho}_{ii\sigma}^{(c)}(\omega)$  where  $f(\epsilon)$  is the Fermi distribution function. The density of states  $\rho_{ij\sigma}^{(c)}(\epsilon)$  is defined by

$$\tilde{\rho}_{ij\sigma}^{(c)}(\epsilon) = -\frac{1}{\pi} \text{Im} [(\tilde{\mathbf{F}}(z)^{-1} + \tilde{\Sigma}^{(c)}(z))^{-1}]_{ij\sigma}, \quad (21)$$

$$(\tilde{\mathbf{F}}(z))_{ij\sigma} = \int \frac{\rho_{ij}(\epsilon) d\epsilon}{z - \epsilon_\sigma - \tilde{\Sigma}_\sigma(z) - \epsilon}, \quad (22)$$

where  $\epsilon_\sigma = \epsilon_0 - \mu + U \langle n_{i-\sigma} \rangle$ , and  $\rho_{ij}(\epsilon)$  is the density of states for a noninteracting system,

$$\rho_{ij}(\epsilon) = \frac{1}{N} \sum_{\mathbf{k}} \delta(\epsilon - \epsilon_{\mathbf{k}}) \exp[-i\mathbf{k} \cdot (\mathbf{R}_i - \mathbf{R}_j)]. \quad (23)$$

The coherent potential introduced in eq. (6) is determined self-consistently from the CPA equation, i.e.,

$$\tilde{\Sigma}_\sigma(z) = \Lambda_{ii\sigma}(z) = N^{-1} \sum_k \Lambda_{k\sigma}(z). \quad (24)$$

Equations (3), (7), (8), (15), and (24) form a self-consistent set of equations from which we can obtain the effective medium  $\tilde{\Sigma}_\sigma(z)$ . The nonlocal excitations are then obtained from eq. (2). We have solved the self-consistent equations at zero temperature within the two-site approximation in which we take into account the first two terms of the right hand side of eq. (7) and the first term in eq. (8).

### 3. Numerical results

#### 3.1 Nonlocal excitations of the half-filled band

The 2D Hubbard model is considered to be an antiferromagnetic insulator with the Néel temperature  $T_N = 0$  K at half filling.<sup>7</sup> In the effective medium approach there are two solutions found, a nonmagnetic solution and an antiferromagnetic (AF) one. The latter describes the system at half filling. But in the SCPM an AF effective medium overestimates antiferromagnetic correlations at

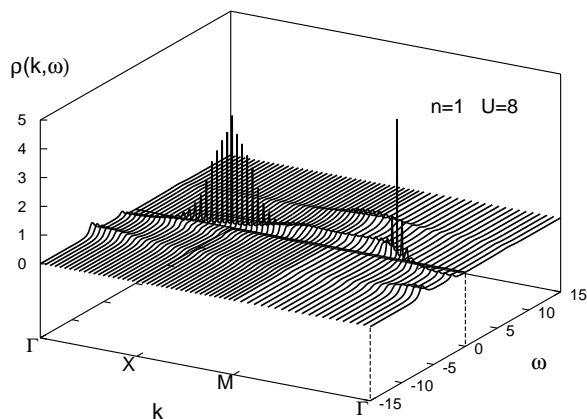


Fig. 1. Single-particle excitation spectrum along the high symmetry lines for half filling ( $n = 1$ ) and  $U = 8$ . The Fermi level is indicated by a bold line. Here and in the followings, the energy is measured in unit of  $|t|$ . Note that  $\Gamma = (0, 0)$ ,  $X = (\pi, 0)$ ,  $M = (\pi, \pi)$  are in unit of the lattice constant.

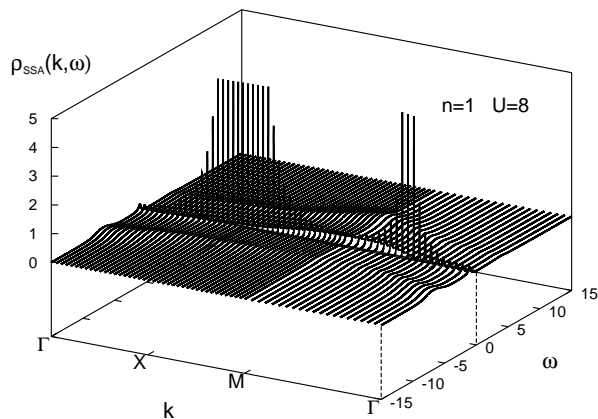


Fig. 2. Single-particle excitation spectra in the single-site approximation (SSA). Parameters are the same as in Fig. 1.

finite doping concentrations because the medium eliminates spin fluctuations. Therefore the SCPM does not describe properly the AF at  $T = 0$ . Here we study the properties of excitations in the presence of the nonmagnetic medium, because the nonmagnetic solution at half-filling is smoothly connected to that at finite doping concentration. In the following we present results for the nonlocal excitations in the nonmagnetic medium at half-filling.

For the numerical calculations, we adopted a  $160 \times 160$  (or  $80 \times 80$ ) mesh in the first Brillouin zone, and obtained the momentum dependent self-energy (3) by taking into account the off-diagonal memory functions up to the 50th (!) nearest neighbors. The latter are calculated from eq. (15). The screened memory functions  $M_{0ij\sigma}^{(c)}(z)$  in eq. (15) are calculated by means of the Laplace transformation method.<sup>39</sup> In order to avoid singularities in the Green functions, we used a complex energy  $z = \omega + i\delta$  with

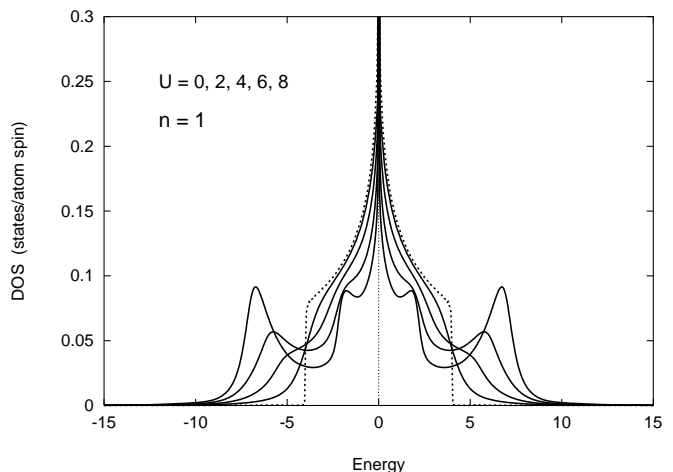


Fig. 3. Total densities of states (DOS) at half filling as function of  $U$ . Noninteracting DOS is shown by dotted line.

$\delta = 0.025$  (or  $\delta = 0.05$ ) in unit of  $|t|$ .

Figure 1 shows the excitation spectrum along the high symmetry line at  $U = 8$ . The spectrum is characterized by incoherent Mott-Hubbard excitations, i.e., a lower Hubbard band (LHB) around the  $\Gamma$  point and an upper Hubbard band (UHB) around the  $M$  point. In addition there is the quasiparticle band near the Fermi energy ( $\omega = 0$ ). The nonlocal excitation spectrum is compared with that in the single-site approximations (see Fig. 2). We find that nonlocal correlations reduce the amplitude of the quasiparticle peak near the Fermi level, and increase its band width by a factor of two as compared with the SSA for an intermediate strength of the repulsion  $U$ . Alternatively, the electron correlations in the SSA overestimate the band narrowing in the quasiparticle state. When intersite correlations are additionally included, the electrons recover parts of the original degrees of freedom for their motion. The result is a band broadening but the Coulomb repulsion energy remains optimized.

Nonlocal excitations also enhance the amplitude of the LHB around the  $\Gamma$  point as well as that of the UHB around the  $M$  point. Similar global features of these nonlocal excitation spectra are also found in the 3D Hubbard model on a simple-cubic lattice.<sup>17</sup> Another characteristic of the spectra is pronounced flat-band excitations at  $\omega \approx \pm 2.0$  due to antiferromagnetic correlations. These flat bands are precursors of an antiferromagnetic insulator.<sup>12</sup> They should develop further when higher-order cluster correlations are taken into account by going beyond the two-site approximation.

The total density of states (DOS) as a function of interaction  $U$  is presented in Fig. 3. A characteristic feature of the DOS is a logarithmic divergence at  $\omega = 0$ , which is due to a van Hove singularity at the  $X$  point. For a small Coulomb interaction, we can compare our results with those of the perturbation theory.<sup>40,41</sup> We find a good agreement between the present DOS and that obtained by the 4th order perturbation theory for  $U = 2$ . For  $U = 4$ , the shoulder position is  $|\omega| = 5.0$  in the present calculation, while it is  $|\omega| = 4.5$  in the 4th order perturbation. These results verify the validity of our

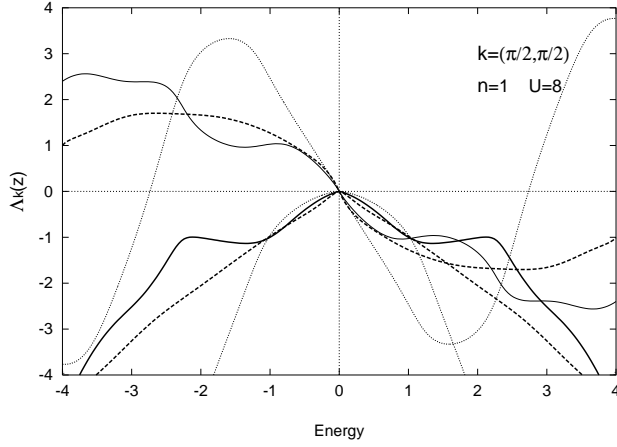


Fig. 4. Self-energies at the Fermi momentum  $(\pi/2, \pi/2)$  in various approximations; Two-site approximation (solid curves), second-order perturbation (thick dashed curves), single-site approximation (thin dashed curves). Note that the real part is antisymmetric, and the imaginary part is symmetric in energy.

results for the regime of Coulomb interaction  $U \lesssim 4$ , in which the 4th order perturbation is believed to be valid. The quasiparticle band in the low energy region becomes narrow when the interaction  $U$  is increased. The Mott-Hubbard incoherent bands on the other hand develop in the high energy regions. Furthermore, the nonlocal antiferromagnetic correlations create subbands at  $|\omega| \approx 1.8$  when  $U \gtrsim 6$ . When  $U \gtrsim 10$ , we find within the two-site approximation a negative spectral density in a small region of momentum space. Therefore we have to include higher-order cluster correlations in order to discuss the spectra beyond  $U \gtrsim 10$  within the present scheme. In the following we limit our discussions to the metallic region  $U \lesssim 10$ .

A characteristic feature of the 2D Hubbard model at half filling is that of marginal Fermi liquid. The MFL is defined by  $\text{Re } \Lambda_{k_F}(z) \propto \omega \ln|\omega|$  and  $\text{Im } \Lambda_{k_F}(z) \propto |\omega|$  for small  $|\omega|$  and for the Fermi wave number  $k_F$ . In the weakly correlated regime such behavior is found by 2nd-order perturbation theory.<sup>38,39</sup> For the intermediate Coulomb interaction strength, we have calculated the self-energy at the Fermi surface. An example is shown in Fig. 4. The MFL behavior seems to be for  $k$  present even for strong Coulomb interaction  $U$ , although numerically the linear dependence of  $\text{Im } \Lambda_{k_F}(z)$  on  $|\omega|$  is not so accurate.

We have calculated the momentum dependent effective mass  $m_k = (1 - \partial \text{Re} \Lambda_k(z) / \partial \omega)_{\omega=0}$  using numerical differentiation. As presented in Fig. 5, the calculated effective mass shows a strong momentum dependence, having a minimum at the M point ( $= (\pi, \pi)$ ), and a maximum at the X point ( $= (\pi, 0)$ ). Along the Fermi surface  $\cos k_x + \cos k_y = 0$ ,  $m_k$  has a minimum at  $(\pi/2, \pi/2)$  and a maximum at  $(\pi, 0)$ . This suggests the appearance of the 'Fermi arc'<sup>42</sup> when holes are doped.

Because  $\text{Re} \Lambda_k(z) \propto \omega \ln|\omega|$  for small  $|\omega|$  in the MFL, it is  $m_k - 1 \propto -\ln \delta\omega$  for small energy steps  $\delta\omega$  when a numerical differentiation is done. Therefore, the simple numerical method for the calculation of  $k$ -dependent ef-

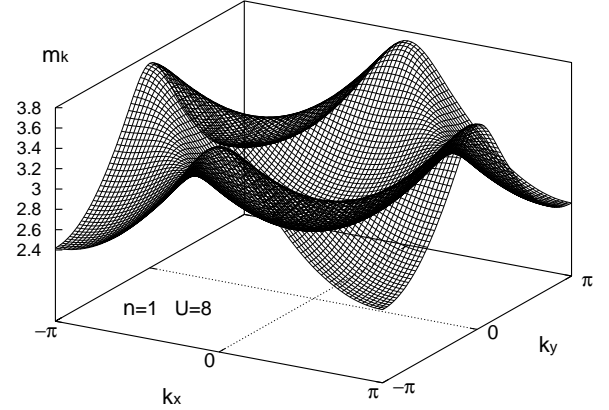


Fig. 5. Momentum dependent effective mass at half filling, calculated by numerical differentiation by using an energy interval of  $\delta\omega = 0.05$ .

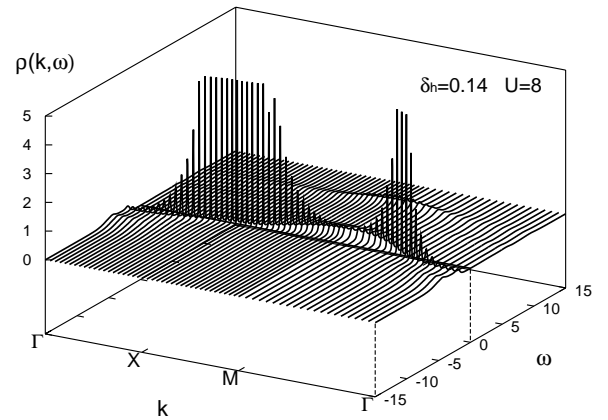


Fig. 6. Excitation spectrum along the high symmetry lines for doping concentration  $\delta_h = 0.14$ .

fective mass breaks down in the case of the MFL. We have verified that the effective mass at the Fermi surface in Fig. 5 increases logarithmically with decreasing  $\delta\omega$ , i.e.,  $m_k$  along the Fermi surface is expected to show a logarithmic divergence. We will return to this problem in Sec. III C.

### 3.2 Nonlocal excitations in the doped Hubbard model

When holes are doped into a half-filled 2D Hubbard system, quantum spin and charge fluctuations are enhanced due to a motion of holes, and thus the system is expected to lose the long range magnetic order. In the very weak Coulomb interaction limit, it is suggested by using the Hartree-Fock approximation<sup>44</sup> that an incommensurate antiferromagnetic order can remain even at finite doping concentration, and the insulating state can survive under the long range magnetic order. A problem of the theory is that a finite value of  $T_N$  at half-filling contradicts with the Mermin-Wagner theorem.<sup>7</sup> This sug-

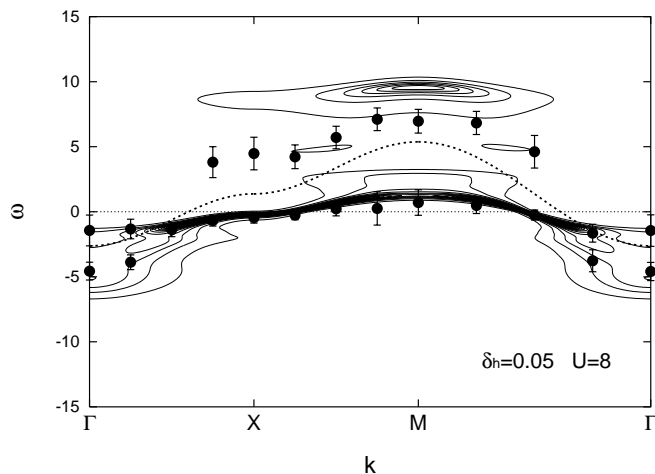


Fig. 7. Contour map of the excitations at  $\delta_h = 0.05$ . Closed circles with error bars are the QMC results<sup>10</sup> at  $T = 0.33$ . The dashed curves show the Hartree-Fock quasiparticle dispersion.

gests that the quantum fluctuations are dominant in the 2D system so that the long range magnetic order is suppressed at finite doping concentration. Although there are no rigorous results on this problem we assume here in our numerical calculations the nonmagnetic state even for an infinitesimal doping concentration.

A typical excitation spectrum is shown in Fig. 6 for a doping concentration of  $\delta_h = 0.14$ . As seen from the figure, the upper Hubbard band moves upwards. The lower Hubbard band has become weaker and merges with the quasiparticle band near the  $\Gamma$  point. The excitations due to short-range AF correlations, which are located at  $|\omega| \approx 1.8$  in Fig. 1, have disappeared. Consequently, the spectral weight of quasiparticle peak is enhanced.

We have examined the doping dependence of the excitation spectra. At 5 % doping, the LHB is nearly destroyed as shown in Fig. 7. The flat bands at  $|\omega| \sim 2$  around the  $\Gamma$  and M point, which are due to short-range antiferromagnetic correlations, have been weakened. The quasiparticle band on the other hand is well developed. Accordingly, the flat quasiparticle band around the X point sinks below the Fermi level. In the optimum doped region (see Fig. 8), the quasiparticle band is further pronounced. But its width is broadened by 26 % as compared with 5 % doping. Note that due to the increase of holes the flat band around the X point is at the Fermi level. In the overdoped region (see Fig. 9), the quasiparticle band gains further weight and its width increases by 10 % as compared with 14 % doping. The flat band around the X point is now above the Fermi level.

We have compared our results at zero temperature with those of the QMC at finite temperatures.<sup>10</sup> As shown by closed circles in Figs. 7, 8, and 9, the present results for the nonlocal excitations are consistent with the QMC results for the underdoped region as well as for the overdoped one. Especially, the calculated quasiparticle bands show quantitative agreement in both cases. In the QMC calculations for 20 % doping concentration, weak excitations are found at  $\omega \approx -3.0$  around the X and  $(\pi/2, \pi/2)$  points as shown in Fig. 9. Although not



Fig. 8. Contour map of the excitations at  $\delta_h = 0.14$ .

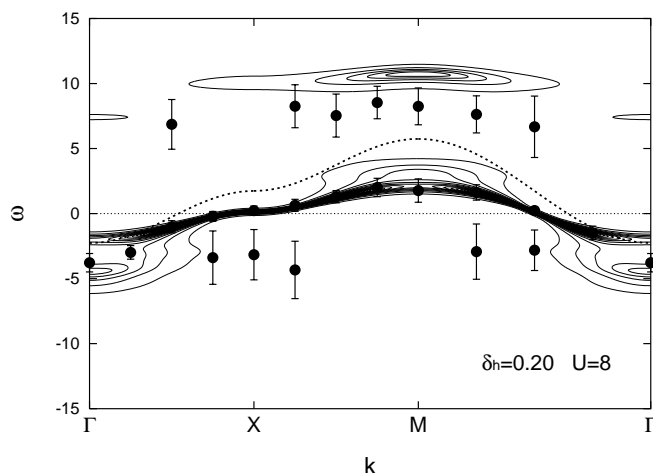


Fig. 9. Contour map of excitation spectra at  $\delta_h = 0.20$ .

visible in Fig. 9, we have verified that the same excitations do appear in our calculations. For example, we find a small peak of height 0.03 at the X point  $(\pi, 0)$  and energy  $\omega = -2.9$ , in agreement with the QMC results. We have also investigated the spectra in the SSA. The quasiparticle weight in the SSA is underestimated at the  $\Gamma$  point and is overestimated at the M point. The LHB (UHB) in the SSA is correspondingly excessively enhanced (weakened).

The integrated DOS's are shown in Fig. 10 for different hole dopings  $\delta_h = 0.05, 0.14, \text{ and } 0.20$ . We find that the weight of the LHB is rather small for these doping concentrations. The upper Hubbard band simply shifts to the higher energy region with increasing doping concentration. The sharp quasiparticle peak near the Fermi level is well developed. The peak first sinks and gradually rises with increasing doping concentration. This behavior is directly connected with the change of the flat band near the X point with hole doping.

We have also investigated the excitation spectrum at  $\omega = 0$ . Results are shown in Figs. 11 and 12. We find a hole-like Fermi surface in the underdoped region and an electron-like Fermi surface in the overdoped region. This

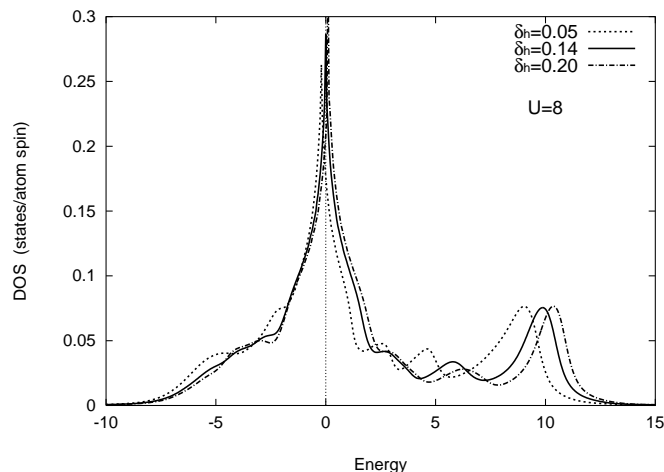
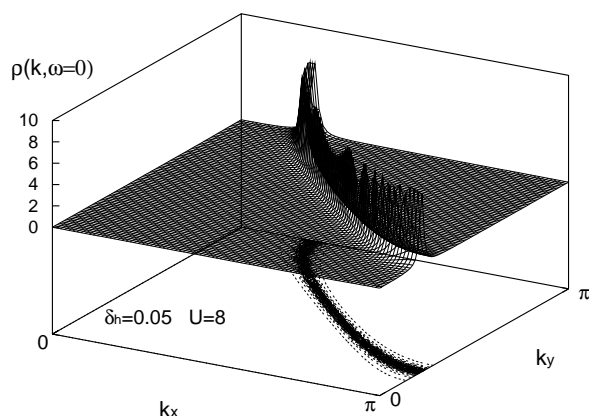


Fig. 10. Total DOS for various doping concentrations

Fig. 11. Excitation spectrum at the Fermi energy for  $\delta_h = 0.05$ .

behavior is in agreement with the one obtained by the dynamical cluster approximation at finite temperatures.<sup>13</sup> It should be noted that the present results do not satisfy Luttinger's theorem.<sup>43</sup> The deviation from the volume predicted by that theorem is small in the overdoped region, but it is large in the underdoped region. The ratio of the excess volume to the predicted one is  $\delta v/v_0 = 0.3$  at  $\delta_h = 0.05$ , for example. It is comparable to the value of 0.4 obtained by the QMC calculations.<sup>10</sup>

The momentum distributions  $n_k$  along the high symmetry lines are presented in Fig. 13. At the M point  $n_k$  decreases with hole doping as expected. The momentum distribution at the  $\Gamma$  point, on the other hand, decreases first and then gradually increases with hole doping. The reduction in the underdoped region originates from the reduction of the LHB as seen in Fig. 10. It also yields an enhancement of  $n_k$  at the X point. It should be noted that there is no jump of  $n_k$  at the X point for half-filling because the quasiparticle weight vanishes there as will be discussed in the next section. It is also interesting that no discontinuity of  $n_k$  is seen at the X point for  $\delta_h = 0.14$  at which the Fermi surface is not well defined because the

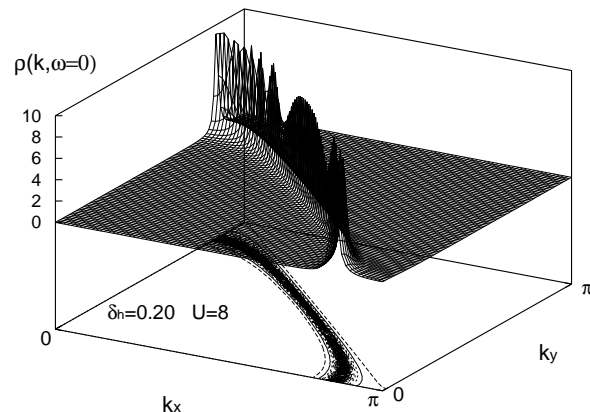
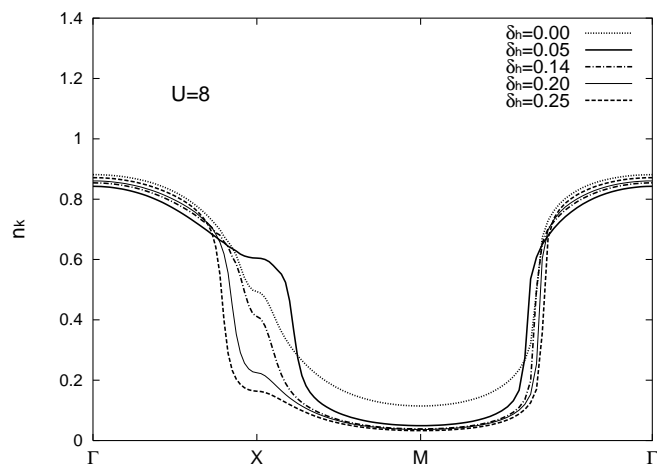
Fig. 12. Excitation spectrum at the Fermi energy for  $\delta_h = 0.20$ .

Fig. 13. Momentum distribution along the high symmetry directions for various doping concentrations.

flat band is here right at the Fermi level. These anomalies are not found along the  $\Gamma$ -M line; we find there a clear discontinuity of  $n_k$  at the Fermi surface irrespective of the doping concentration.

### 3.3 Marginal Fermi liquid behavior

We have discussed in Sec. III A the strong  $k$  dependence of the effective mass  $m_k$  and we have pointed out its logarithmic divergence at the Fermi level for the case of half filling (see Fig. 5). When holes are doped, the effective mass rapidly loses the  $k$  dependence. We show in Fig. 14 an example for 5% doping, where the maximum of  $m_k$  changes from the X point to the  $\Gamma$  point. The maximum and minimum values of  $m_k$  with increasing doping concentration are shown in Fig. 15. Both quantities increase with decreasing doping concentration. At  $\delta_h^* = 0.025$ , we find a sudden change of  $m_k$ . When the energy in the numerical differentiation is changed in steps varying from  $\delta\omega = 0.05$  to  $\delta\omega = 0.005$ , the maximum value of  $m_k$  at the X point increases logarithmically for  $\delta_h < \delta_h^*$  as shown in Fig. 15. This implies that up to the finite doping concentrations of 2.5% the electrons are

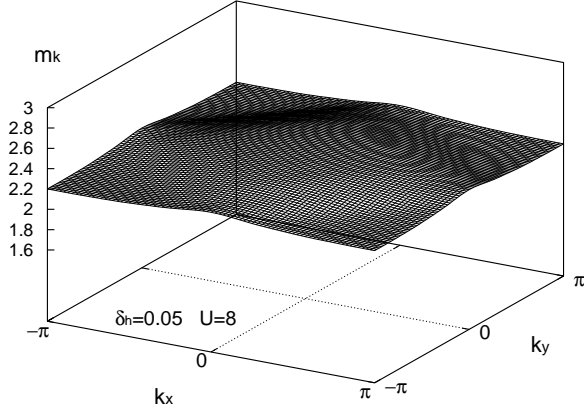
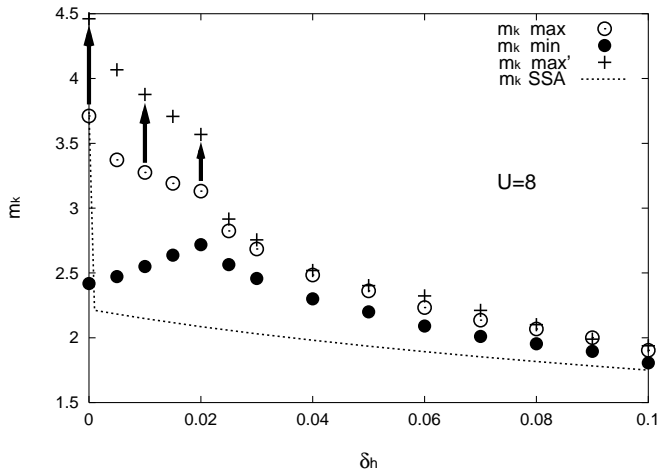
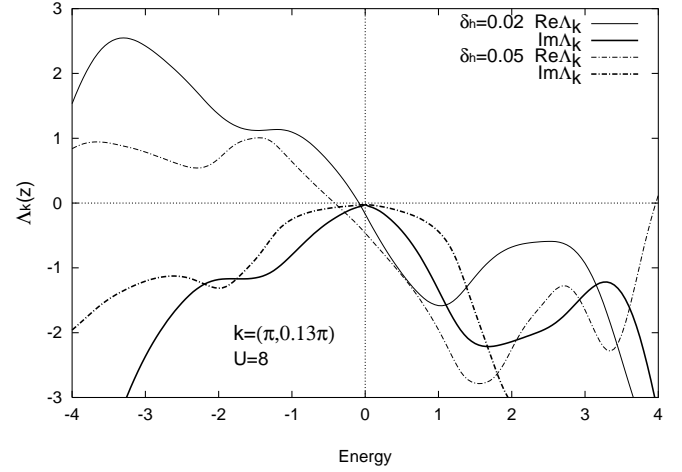
Fig. 14. Momentum-dependent effective mass for  $\delta_h = 0.05$ .

Fig. 15. Momentum-dependent effective mass  $m_k$  vs. doping concentration  $\delta_h$ . Open circles: maximum value at the X point for  $\delta_h \leq 0.02$  and  $\Gamma$  point for  $\delta_h \geq 0.02$ , closed circles: minimum value at the M point. Numerical derivatives are taken with energy steps of  $\delta\omega = 0.05$ . In the case of maximum  $m_k$ , the results for  $\delta\omega = 0.005$  are shown by +. The momentum-independent effective mass in the single-site approximation (SSA) is shown by the dashed curve.

forming a MFL. We can not verify numerically though *how accurately* a MFL is realized at those concentrations. Figure 16 shows the calculated self-energies at a particular  $\mathbf{k}_F$  for  $\delta_h = 0.02$  (in the MFL region) and  $\delta_h = 0.05$  (in the Fermi liquid region). The  $\text{Im} \Lambda_{k_F}(z)$  at  $\delta_h = 0.02$  is approximately proportional to  $|\omega|$  for small  $\omega$ . We therefore conclude that the quasiparticle states in the low doping region are at least very close to a MFL. We note that a MFL can not be described by the conventional cluster approaches because the long-range intersite correlations near the Fermi surface are indispensable for it to occur and they are not taken into account in the usual cluster theories.

As mentioned before, the change from the Fermi liquid (FL) to the MFL takes place discontinuously. This is clearly seen in the doping dependence of the chemi-

Fig. 16. Self-energy at the Fermi momentum  $\mathbf{k} = (\pi, 0.13\pi)$  for doping concentrations  $\delta_h = 0.02$  and  $0.05$ .

cal potential shown in Fig. 17. The chemical potential increases monotonically with decreasing doping concentration and jumps at  $\delta_h^* = 0.025$  by  $\Delta\mu \simeq 0.55$ . Between  $\delta_h = 0.020$  and  $\delta_h = 0.025$ , we find two solutions. Below  $\delta_h = 0.020$ , there is only one solution corresponding to a MFL.

The discontinuity in the chemical potential as well as in  $m_k$  at  $\delta_h^*$  originates from the collapse of the LHB with increasing hole doping. Figure 18 shows the total DOS at  $\delta_h = 0.02$  and  $0.05$ . At low doping concentrations, the spectral weight of the LHB moves directly to the UHB with increasing doping because doubly occupied states are almost totally suppressed when correlations are strong. Consequently, the van Hove singularity is pinned to the Fermi level as shown in Fig. 18. It leads to the MFL behavior at finite doping concentrations up to 2.5 %. Further doping, however, causes the LHB to disappear and so the peak at the Fermi level, which is associated with a flat band around the X point, is moving down below the Fermi level. Finally, the spectral weight of the LHB moves to the quasiparticle states, and the electrons obtain more and more itinerant character with reduced correlations.

Calculated discontinuity lines in the  $U - \delta_h$  plane are presented in Fig. 19. The MFL-like state with the well-defined LHB is located around  $\delta_h = 0.02$  and  $U = 8$ . The MFL is separated from the normal FL state with collapsed LHB by a hatched region in which two self-consistent solutions exist. Note that the hatched region is slightly reduced as compared with our preliminary result<sup>28</sup> because we have increased the numerical accuracy. We also found two additional discontinuity lines in the  $U - \delta_h$  plane. One is around  $\delta_h = 0.005$  and  $U = 7.5$ , while the other is around  $\delta_h = 0.10$  and  $U = 6.5$ . The discontinuities are small ( $\Delta\mu \sim 0.05$ ) at both lines and the latter changes to the kink-like anomalies which are indicated in Fig. 19 by the dotted lines. We have examined these discontinuities of  $\Delta\mu$  by changing the mesh of  $\omega$  and  $\mathbf{k}$  in the numerical calculations. Our conclusion is that the discontinuity with the hatched region and that around  $(\delta_h, U) = (0.005, 7.5)$  exists. But, for the line



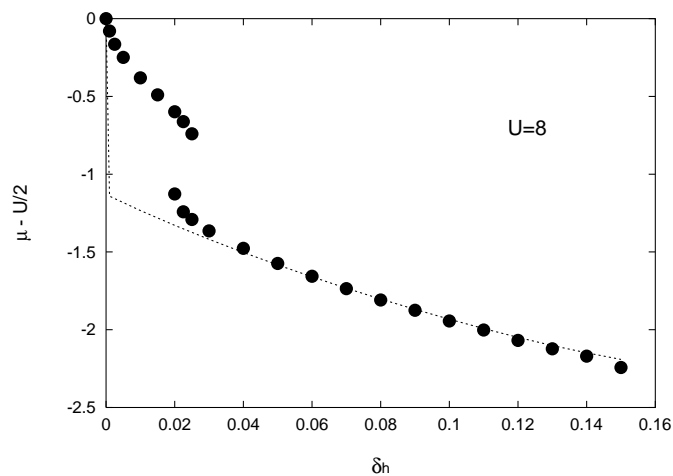


Fig. 17. Chemical potential vs. doping concentration. The dashed curve shows results of the SSA.

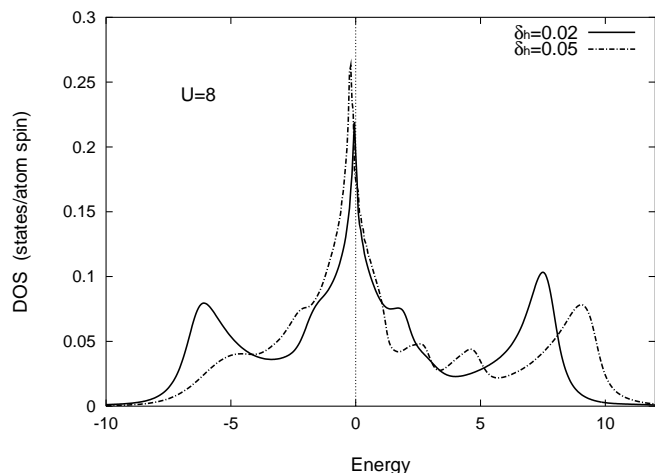


Fig. 18. The DOS of the marginal Fermi liquid like state (solid curve) and the normal Fermi liquid state (dot-dashed curve).

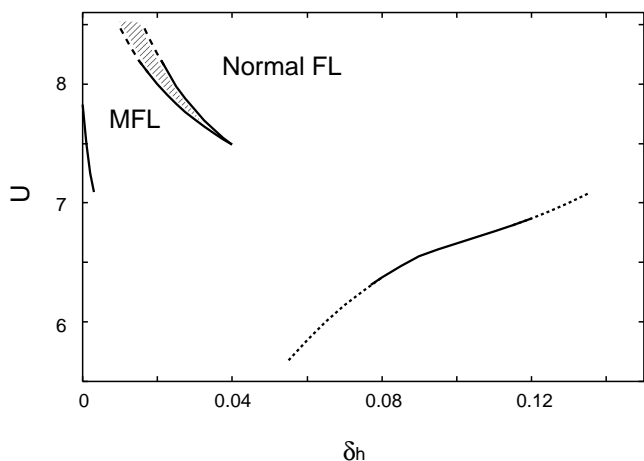


Fig. 19. Phase diagram showing the marginal Fermi liquid regime (MFL) and the normal Fermi liquid state (Normal FL) regime. The lines at which the chemical potential changes discontinuously are shown by solid curves. The region with two self-consistent solutions is shown by the hatched area. Dashed lines along the hatched area are extrapolations. Along the dotted lines the chemical potential has a kink.

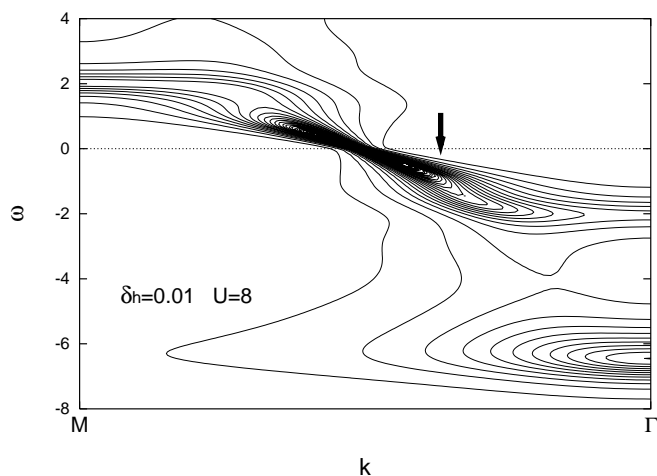


Fig. 20. The excitation spectrum along the nodal direction showing a kink structure for  $\delta_h = 0.01$ . The arrow indicates the kink position  $|\mathbf{k}| = 0.52\pi$ .

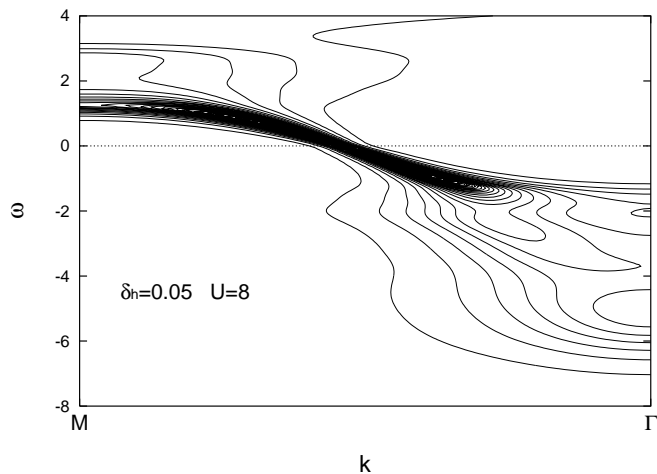


Fig. 21. The excitation spectrum along the nodal direction for  $\delta_h = 0.05$ .

around  $(\delta_h, U) = (0.10, 6.5)$ , the value  $\Delta\mu$  and position seem still to depend on the number of mesh points even when both the momentum steps and the energy steps are decreased down to  $\pi/80$  and 0.025, respectively. Therefore we do not exclude the possibility that the line disappears when the numerical accuracy is increased further.

### 3.4 Kink structure in the underdoped region

We have examined the nonlocal excitations in the MFL region. The excitations in this region are similar to the ones of the half-filled case (see Fig. 1). The LHB excitations are located around the  $\Gamma$  point at  $\omega \approx -6.0$ . We also find flat-band excitations at  $\omega = \pm 2.0$ , which are due to short-range antiferromagnetic correlations. The detailed structure of the quasiparticle states is however unusual. Figure 20 shows a spectrum along the nodal direction for  $\delta_h = 0.01$ . Notice that a kink structure appears in the quasiparticle states at  $(|\mathbf{k}|, \omega) = (0.52\pi, -0.85)$ . The kink is caused by a mixing of quasiparticle states with the excitations due to magnetic short-range order. The

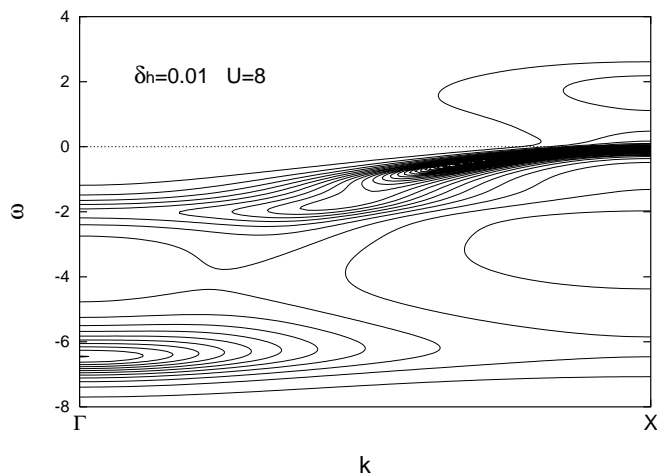


Fig. 22. The excitation spectrum along the antinodal direction for  $\delta_h = 0.01$ .

latter are enhanced by the nesting of the Fermi surface in the MFL region. When  $\delta_h > 0.03$ , the LHB collapses as mentioned before and the flat band around the X point sinks. Accordingly the excitations due to antiferromagnetic correlations are weakened. The quasiparticle state is then extended to the higher energy region and the kink structure disappears as shown in Fig. 21.

We have also examined the quasiparticle excitations along the antinodal direction. As seen in Fig. 22 the mixing of the quasiparticle band with the excitations due to the short-range antiferromagnetic correlations is no longer so strong, and we do not find a clear kink along this direction.

The ratios of the Fermi velocity above the kink energy  $\omega_{\text{kink}}$  to that below the one are  $v_{F'}/v_F = 2.7$  ( $\delta_h = 0.0$ ), 1.8 ( $\delta_h = 0.01$ ), and 1.5 ( $\delta_h = 0.02$ ), respectively. The concentration dependence of the Fermi velocity above  $\omega_{\text{kink}}$  is shown in Fig. 23. Along the  $\Gamma$ -M direction, the Fermi velocity is reduced by a factor of two as compared with the one of the noninteracting system. Its concentration dependence is rather weak. The Fermi velocity along the  $\Gamma$ -X-M line is strongly influenced by the energy position of the flat band at the X point. It first increases with the shift of the Fermi momentum  $\mathbf{k}_F$  towards the M point, then decreases gradually with the return of  $\mathbf{k}_F$  to the X point. When  $\delta_h = 0.14$ ,  $\mathbf{k}_F$  crosses the X point, and the Fermi velocity starts to increase again with hole doping.

#### 4. Summary and discussions

We have investigated numerically the single-particle excitation spectra of the 2D Hubbard model at zero temperature and various doping concentrations, thereby using the self-consistent projection operator method (SCPM). The SCPM describes the nonlocal excitations due to long-range intersite correlations, and allows us to compute the spectra with high energy and momentum resolution. The method therefore is able to clarify details of nonlocal excitations that had not been resolved by previous approaches.

We have calculated the momentum-dependent excita-

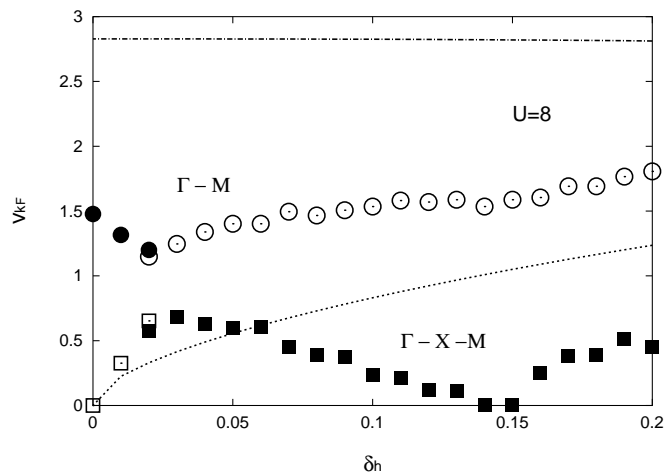


Fig. 23. Fermi velocity along  $\Gamma$ -M (closed circles: the MFL state, and open circles: the FL) and  $\Gamma$ -X-M (open squares: the MFL state, and closed squares: the FL). Corresponding values for the noninteracting system are shown by the dot-dashed curve and dotted curve, respectively.

tion spectra from the underdoped to the overdoped region within the two-site approximation. Pairs of sites, up to the 50th nearest neighbor were considered. The spectra are characterized by a LHB around the  $\Gamma$  point, and an UHB around the M point. They show strongly renormalized quasiparticle states near the Fermi level, as well as excitations caused by magnetic short-range correlations. We verified that the present results are consistent with those obtained by QMC calculations at finite temperatures.<sup>10</sup> Especially the quasiparticle excitations show a quantitative agreement with the QMC results. We have shown that compared with the single-site approximation intersite correlations suppress the quasiparticle weight in the vicinity of the Fermi level by a factor of two. They relax also the band narrowing of quasiparticles by a factor of two for an intermediate strength of the repulsive interaction. Intersite correlations also produce excitations due to short-range antiferromagnetic order in the underdoped region. Around the X point the correlations smoothen a sharp drop of the momentum distribution  $n_k$  at the Fermi surface.

The antibonding band of Cu  $3d_{x^2-y^2}$  orbitals hybridizing with the planar O  $2p_x$  and  $2p_y$  orbitals is approximately described by a 2D Hubbard model.<sup>1, 2, 21</sup> Therefore the present results suggest an explanation of some of the unusual properties in the high  $T_c$  cuprates. We obtained a hole-like Fermi surface for the underdoped region and an electron-like Fermi surface for the overdoped region, being in agreement with the experimental data on LSCO.<sup>45</sup> We found numerically a MFL-like behavior at finite doping concentrations by analyzing the momentum dependence of the effective mass. The results justify a phenomenological MFL description<sup>22</sup> which explains many aspects of the normal state in cuprates. We found that the MFL is caused by a pinning of the van Hove singularity to the Fermi level. It is due to a transfer of spectral weight from the LHB to the UHB for small doping concentrations when  $U/|t|$  is sufficiently large. The

MFL region calculated here is limited to a small area in the  $U/|t|$  vs.  $\delta_h$  plane. It remains work for the future to extend the MFL region by going beyond the two-site approximation and by improving the model.

The present theory yields a large deviation from the Luttinger theorem<sup>43</sup> in the underdoped region in agreement with previous investigations.<sup>10,13</sup> In our calculations, the violation is caused by a sudden reduction of the LHB with increasing doping concentration or Coulomb interaction strength  $U$ . The collapse of the LHB strongly pulls down the flat band around the X point and increases considerably the volume below the Fermi surface. Accordingly, the spectral weight of the LHB moves to a higher energy region. It has not yet been clarified however, under which general conditions the Luttinger theorem can be violated. Experimentally, LSCO has been reported to satisfy Luttinger's theorem,<sup>45</sup> while  $\text{Ca}_{2-x}\text{Na}_x\text{CuO}_2\text{Cl}_2$  was shown to violate it strongly.<sup>45,46</sup> In the latter case, it has been observed that the LHB approaches the Fermi level with hole doping. This might correspond to the collapse of the LHB and the transfer of spectral weight to the higher energy region found in our calculations.

We have also found in the underdoped region a kink in the excitation spectrum along the nodal direction. The kink is caused by a mixing between the quasiparticle band and the excitation band caused by short-range antiferromagnetic correlations. This suggests that the kink found in the cuprate is of electronic origin; in principle there is no need to include any other (e.g. phononic) degrees of freedom coupled to electrons in order to explain the kink structure. In fact, we obtain kink energies of  $\omega_{\text{kink}} = 130\text{-}170$  meV when we adopt a reasonable transfer integral  $|t| = 0.2$  eV.<sup>13</sup> They are comparable to the experimental values of 60-70 meV.<sup>25</sup> Calculated ratios of the Fermi velocity  $v_{F'}/v_F$  at  $\omega_{\text{kink}}$  are between 1.5 and 2.7 in the underdoped region. These values should be compared with the experimental ones,<sup>47</sup> i.e., 1.3-3.0. We suggest that a strong doping dependence of the kink in  $\text{La}_{2-x}\text{Sr}_x\text{CuO}_4$  ( $0 < x < 0.07$ )<sup>47</sup> can be explained by a strong doping dependence of the antiferromagnetic short-range order as found in the present calculations.

The 2D Hubbard model considered here is the simplest model for cuprates. It is leading to a Néel temperature  $T_N = 0$  at half filling. In order to describe the layered Cu-based perovskites with high  $T_N$  we have to adopt more realistic models, i.e., we have to include 3D features. Furthermore the present calculations neglect the self-consistency of the off-diagonal matrix elements of the effective medium. Because of the missing self-consistency, the results presented here may underestimate the antiferromagnetic correlations. The self-consistency of the off-diagonal matrix elements of the effective medium and the higher-order cluster correlations should extend the MFL and the kink region on the phase diagram. Corresponding calculations are left for future investigations.

*Note added in proof*—Recently a high energy anomaly called “waterfall” has been found at about 0.3-0.5 eV in the ARPES of high- $T_c$  cuprates [ W. Meevasana *et.*

*al.*, cond-mat/0612541v1; J. Graf *et. al.*, Phys. Rev. Lett., **98**, (2007) 067004; D.S. Inosov *et. al.*, cond-mat/0703223v1 ]. According to the data on LSCO, the low-energy kink anomaly at 60-70 meV strongly depends on the doping concentration, while the high energy anomaly does not. We suggest that the former corresponds to the kink anomaly we found here because of the strong concentration dependence and that the latter might be a phenomenon related to a mixing between the quasiparticle band and the incoherent LHB.

## Acknowledgment

Numerical calculations have been partly carried out by using the facilities of the Supercomputer Center, Institute for Solid State Physics, University of Tokyo.

- 1) E. Dagotto, Rev. Mod. Phys. **66**, (1994) 763.
- 2) M. Imada, A. Fujimori, and Y. Tokura, Rev. Mod. Phys. **70**, (1998) 1039.
- 3) T. Maier, M. Jarrell, T. Pruschke, M.H. Hettler, Rev. Mod. Phys. **77**, (2005) 1027.
- 4) P.W. Anderson, *The Theory of Superconductivity in the High- $T_c$  Cuprates* (Princeton University Press, Princeton, 1997).
- 5) H.-B. Schüttler and A.J. Fedro, Phys. Rev. B **45**, (1992) 7588.
- 6) M.E. Simon and A.A. Aliga, Phys. Rev. B **48**, (1993) 7471.
- 7) N.D. Mermin and H. Wagner, Phys. Rev. Lett. **17**, (1966) 1133; D.K. Ghosh, Phys. Rev. Lett. **27**, (1971) 1584; *ibid* **28**, (1972) 330.
- 8) N. Bulut, D.J. Scalapino, and S.R. White, Phys. Rev. Lett **73**, (1994) 748; **72**, (1994) 705; Phys. Rev. **50**, (1994) 7215.
- 9) R. Preuss, W. Hanke, and W. von der Linden, Phys. Rev. Lett **75**, (1994) 1344.
- 10) C. Gröber, R. Eder, and W. Hanke, Phys. Rev. **B62**, (2000) 4336.
- 11) N. Furukawa and M. Imada, J. Phys. Soc. Jpn. **61**, (1992) 3331.
- 12) M. Jarrell, Th. Maier, C. Huscroft, and S. Moukouri, Phys. Rev. B **64**, (2001) 195130.
- 13) Th. A. Maier, Th. Pruschke, and M. Jarrell, Phys. Rev. **B66**, (2002) 075102.
- 14) M. Jarrell, Th. Maier, M.H. Hettler and A.N. Tahvildarzadeh, Europhys. Lett. **56**, (2001) 563.
- 15) Y. Takehashi, Adv. Phys. **53**, (2004) 497.
- 16) P.D. Johnson, T. Valla, A.V. Fedorov, Z. Yusof, B.O. Wells, Q. Li, A.R. Moodenbaugh, G.D. Gu, N. Koshizuka, C. Kendziora, Sha Jian, and D.G. Hinks, Phys. Rev. Lett. **87**, (2001) 177007.
- 17) Y. Takehashi and P. Fulde, Phys. Rev. **B70**, (2004) 195102.
- 18) Y. Takehashi and P. Fulde, Phys. Rev. **B69**, (2004) 045101; Phys. Rev. **B70**, (2004) 155112.
- 19) H. Stoll, Phys. Rev. B **46**, (1992) 6700; Chem. Phys. Lett. **191**, (1992) 548.
- 20) P. Fulde, Adv. in Phys. **51**, (2002) 909.
- 21) M.R. Norman and C. Pépin, Rep. Prog. Phys. **66**, (2003) 1547.
- 22) C.M. Varma, P.B. Littlewood, and S. Schmitt-Rink, E. Abrahams, and A.E. Ruckenstein, Phys. Rev. Lett. **63**, (1989) 1996; E. Abrahams and C.M. Varma, Phys. Rev. **B68**, (2003) 094502.
- 23) P.V. Bogdanov, A. Lanzara, S.A. Keller, X.J. Zhou, E.D. Lu, W.J. Zheng, G. Gu, J.-I. Shimoyama, K. Kishio, H. Ikeda, R. Yoshizaki, Z. Hussain, and Z.X. Shen: Phys. Rev. Lett. **85** (2000) 2581.
- 24) A. Lanzara, P.V. Bogdanov, X.J. Zhou, S.A. Keller, D.L. Feng, E.D. Lu, T. Yoshida, H. Eisaki, A. Fujimori, K. Kishio, J.-I. Shimoyama, T. Noda, S. Uchida, Z. Hussain, Z.-X. Shen: Nature **412** (2001) 510.
- 25) T. Cuk, D.H. Lu, X.J. Zhou, Z.-X. Shen, T.P. Devereaux, and N. Nagaosa: phys. stat. sol. (b) **242** (2005) 11.
- 26) M. Eschrig and M.R. Norman: Phys. Rev. Lett. **85**, (2000) 3261; Phys. Rev. Lett. **89**, (2002) 277005.
- 27) E. Schachinger, J.J. Tu, and J.P. Carbotte: cond-mat/0304029.
- 28) Y. Takehashi and P. Fulde, Phys. Rev. Lett. **94**, (2005) 156401.

- 29) Y. Kakehashi and P. Fulde, J. Phys. Soc. Jpn. **74**, (2005) 2397.
- 30) See for example, P. Fulde, *Electron Correlations in Molecules and Solids* (Springer, Berlin, 1995).
- 31) W.D. Lukas and P. Fulde, Z. Phys. B **48**, (1982) 113.
- 32) R. Kishore, Phys. Rev. B **35**, (1987) 6854.
- 33) S. Hirooka and M. Shimizu, J. Phys. Soc. Jpn. **43**, (1977) 70.
- 34) Y. Kakehashi, Phys. Rev. B **45**, (1992) 7196; Phys. Rev. B **65**, (2002) 184420.
- 35) A. Georges, G. Kotliar, W. Krauth, and M. J. Rosenberg, Rev. Mod. Phys. **68**, (1996) 13.
- 36) Y. Kakehashi, Phys. Rev. B **66**, (2002) 104428.
- 37) We adopted here the self-energy with parameters  $(\lambda, \lambda') = (0, 1)$  in eq. (53) of ref.,<sup>17</sup> because we verified in infinite dimensions that this choice of parameters yields a reasonable results near the half filling.
- 38) A. Virosztek and J. Ruvalds, Phys. Rev. B **42**, (1990) 4064.
- 39) H. Schweitzer and G. Czycholl, Z. Phys. B **83**, (1991) 93.
- 40) V. Zlatić, B. Horvatić, B. Dolićki, S. Grabowski, P. Entel, and K.-D. Schotte, Phys. Rev. B. **63**, (2000) 035104.
- 41) S. Shinkai, H. Ikeda, and K. Yamada, J. Phys. Soc. Jpn. **74**, (2005) 2592; H. Ikeda, J. Magn. Magn. Mater., to be published.
- 42) T. Yoshida, X.J. Zhou, T. Sasagawa, W.L. Yang, P.V. Bogdanov, A. Lanzara, Z. Hussain, T. Mizokawa, A. Fujimori, H. Eisaki, Z.-X. Shen, T. Kakeshita, and S. Uchida, Phys. Rev. Lett. **91**, (2003) 027001.
- 43) J.M. Luttinger and J.C. Ward, Phys. Rev. **118**, (1960) 1417.
- 44) H.J. Schulz, Phys. Rev. Lett. **64**, (1990) 1445.
- 45) T. Yoshida, X.J. Zhou, K. Tanaka, W.L. Yang, Z. Hussain, Z.-X. Shen, A. Fujimori, S. Komiya, Y. Ando, H. Eisaki, T. Kakeshita, and S. Uchida, cond-mat/0510608.
- 46) K.M. Shen, F. Ronning, D.H. Lu, F. Baumberger, N.J.C. Ingle, W.S. Lee, M. Meevasana, Y. Kosaka, M. Azuma, M. Takano, H. Takagi, Z.-X. Shen, Science **307**, (2005) 901.
- 47) X.J. Zhou, J. Shi, T. Yoshida, T. Cuk, W.L. Yang, V. Brouet, J. Nakamura, N. Mannella, S. Komiya, Y. Ando, F. Zhou, W.X. Ti, J.W. Xiong, Z.X. Zhao, T. Sasagawa, T. Kakeshita, E. Eisaki, S. Uchida, A. Fujimori, Z. Zhang, E.W. Plummer, R.B. Laughlin, Z. Hussain, and Z.-X. Shen, Phys. Rev. Lett. **95**, (2005) 117001.